Inorganic Chemistry
Article

Inorg. Chem. **2010**, *49*, 6565–6574 **6565**
DOI: 10.1021/ic100500p

Carboxylate Tolerance of the Redox-Active Platform [Ru(μ-tppz)Ru]^n, where tppz = 2,3,5,6-Tetrakis(2-pyridyl)pyrazine, in the Electron-Transfer Series [(L)ClRu(μ-tppz)RuCl(L)]^n, n = 2+, +, 0, −, 2−, with 2-Picolinato, Quinaldato, and 8-Quinolinecarboxylato Ligands (L^-)

Tanaya Kundu,[†] Biprajit Sarkar,[‡] Tapan Kumar Mondal,[§] Jan Fiedler,[⊥] Shaikh M. Mobin,[†] Wolfgang Kaim,*[,‡] and Goutam Kumar Lahiri*[,†]

[†]*Department of Chemistry, Indian Institute of Technology Bombay, Powai, Mumbai 400076, India,* [‡]*Institut für Anorganische Chemie, Universität Stuttgart, Pfaffenwaldring 55, D-70550 Stuttgart, Germany,* [⊥]*J. Heyrovský Institute of Physical Chemistry, v.v.i., Academy of Sciences of the Czech Republic, Dolejškova 3, CZ-18223 Prague, Czech Republic, and* [§]*Department of Chemistry, Jadavpur University, Jadavpur, Kolkata 700032, India*

Received March 16, 2010

The neutral title complexes [(L_{1-3})ClRu^{II}(μ-tppz)Ru^{II}Cl(L_{1-3})] [tppz = 2,3,5,6-tetrakis(2-pyridyl)pyrazine with L_1 = 2-picolinate, L_2 = 2-quinolinecarboxylate (quinaldate) and with the hitherto little used L_3 = 8-quinolinecarboxylate] have been structurally characterized as approximately anti- (**1** and **3**) and syn-configured isomers (**2**) with L ligand N (**1** and **3**) or O atoms (**2**) trans to the pyrazine N atoms of tppz. In contrast to **1** and **2** with five-membered chelate rings, complex **3** (which is isomeric with **2**) contains six-membered chelate rings. Each system **1**−**3** thus features a significantly different coordination situation, and all complexes exhibit a considerably distorted tppz bridge, including a twisted central pyrazine ring. In spite of this, double one-electron reduction of the bridge is always possible, as is evident from electron paramagnetic resonance (EPR) and UV/vis spectroelectrochemistry. Two separate ($\Delta E \sim 0.4$ V and $K_c \sim 10^7$) one-electron oxidations occur on the metals, producing invariably EPR-silent (4 K) Ru^{III}Ru^{II} intermediates with moderately intense near-IR absorptions, ranging from 1500 to 1900 nm. IR spectroelectrochemistry of the carboxylato carbonyl stretching bands did not result in any noticeable shift, in contrast to what was observed with dipyridyl ketones and related coligands. Density functional theory (DFT)/time-dependent DFT calculations confirm the experimental structures and explain the noted spectroscopic trends: destabilized and closer-spaced frontier orbitals for **3** over **2**, with the comparison to **1** suggesting that the configuration is a major factor. Nevertheless, the rather unperturbed electronic structure of the [Ru(μ-tppz)Ru]^n entity, despite different coordination situations at the metal sites, is remarkable and suggests further use of this entity as a robust, carboxylate-tolerant redox-active platform in extended frameworks.

Introduction

The establishment of pyrazine-mediated intramolecular electron transfer in the mixed-valent Ru^{III}Ru^{II} states of the Creutz−Taube ion (**A**)[1] and of its cyano analogue (**B**)[2] has initiated continuous efforts to understand the valence localization/delocalization phenomena in mixed-valent diruthenium complexes, using a variety of pyrazine-derived bridging ligands.[3] Theoretical,[4] methodical,[5] and conceptual advances have been made.[6] The molecular bridge-mediated electronic interaction between redox-active transition-metal ions has significantly contributed to a general understanding of the redox reactivity[3t,u,6] and to speculation about its potential applications in information transfer[7] and energy-relevant research.[8]

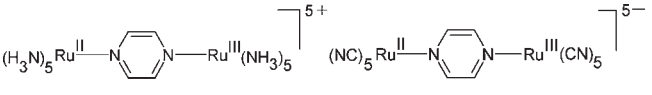

A **B**

In the context of the suitability of pyrazines and other 1,4-diazines as electron-transfer-supporting bridging systems,[9] the potential of the bis-tridentate, redox noninnocent, and inherently nonplanar bridging ligand 2,3,5,6-tetrakis(2-pyridyl)pyrazine (tppz) toward electron-transfer between mixed-valent diruthenium termini containing ancillary ligands

*To whom correspondence should be addressed. E-mail: kaim@iac.uni-stuttgart.de (W.K.), lahiri@chem.iitb.ac.in (G.K.L.).

(1) (a) Creutz, C.; Taube, H. *J. Am. Chem. Soc.* **1969**, *91*, 3988. (b) Creutz, C.; Taube, H. *J. Am. Chem. Soc.* **1973**, *95*, 1086.

(2) Scheiring, T.; Kaim, W.; Olabe, J. A.; Parise, A. R.; Fiedler, J. *Inorg. Chim. Acta* **2000**, *125*, 300.

Published on Web 06/17/2010

(ALs) having varying electronic properties has been explored in recent years (Scheme S1 in the Supporting Information, SI).[10] The low-lying empty π^* orbital of the central pyrazine ring, even in the typically[10f,g,m,n] nonplanar conformation of coordinated tppz, was found to be an efficient mediator for intramolecular electron-transfer processes, and the resulting complexes have shown appreciable variations in the extent of electrochemical coupling (K_c) primarily based on the ALs.[10]

The present work aims to investigate the influence of ALs, 2-picolinato (L_1^-) and isomeric 2- and 8-quinolinecarboxylato (L_2^- and L_3^-), on the molecular geometry and electronic properties of $[\{(L_{1-3})ClRu\}_2(\mu\text{-tppz})]^n$ (**1**−**3**).

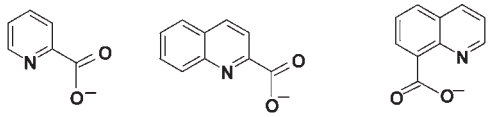

2-picolinate quinaldate 8-quinoline carboxylate

2-Picolinate and quinaldate are involved in the metabolism of tryptophan,[11a] and chromium picolinate is considered to be biorelevant.[11b] Biosensor[12a] and catalysis applications were discussed for complexes of L_1^- and L_2^- with ruthenium,[12b,c] but only a few structurally characterized complexes of this metal with L_1^{-13} and L_2^{-14} were reported.

Herein we describe the synthesis and structural characterization of **1**−**3**. The effect of the structural variety of L_1^-−L_3^- on the electronic properties of $\mathbf{1}^n$−$\mathbf{3}^n$ (n = 2+ to 2−) has been analyzed by experimental and density functional theory (DFT) calculations.

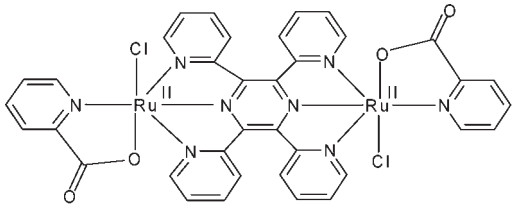

1

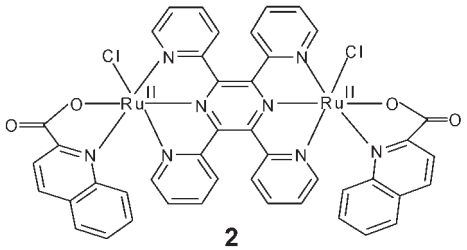

2

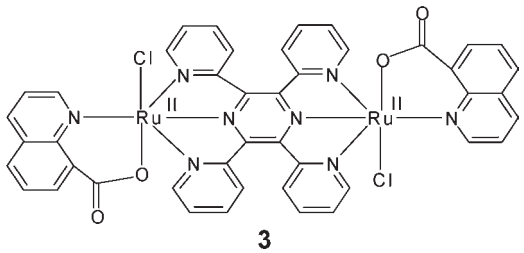

3

(3) (a) Rillema, D. P.; Mack, K. B. *Inorg. Chem.* **1982**, *21*, 3849. (b) Braunstein, C. H.; Baker, A. D.; Strekas, T. C.; Gafney, H. D. *Inorg. Chem.* **1984**, *23*, 857. (c) Ruminski, R. R.; Cockroft, T.; Shoup, M. *Inorg. Chem.* **1988**, *27*, 4026. (d) Balzani, V.; Juris, A.; Venturi, M.; Campagna, S.; Serroni, S. *Chem. Rev.* **1996**, *96*, 759. (e) Gourdon, A.; Launay, J.-P. *Inorg. Chem.* **1998**, *37*, 5336. (f) Bonhote, P.; Lecas, A.; Amouyal, E. *Chem. Commun.* **1998**, 885. (g) Denti, G.; Campagna, S.; Sabatino, L.; Serroni, S.; Ciano, M.; Balzani, V. *Inorg. Chem.* **1990**, *29*, 4750. (h) Stadler, A.-M.; Puntoriero, F.; Campagna, S.; Kyritsakas, N.; Welter, R.; Lehn, J.-M. *Chem.—Eur. J.* **2005**, *11*, 3997. (i) Browne, W. R.; O'Boyle, N. M.; Henry, W.; Guckian, A. L.; Horn, S.; Fett, T.; O'Connor, C. M.; Duati, M.; Cola, L. D.; Coates, C. G.; Ronayne, K. L.; McGarvey, J. J.; Vos, J. G. *J. Am. Chem. Soc.* **2005**, *127*, 1229. (j) D'Alessandro, D. M.; Topley, A. C.; Davies, M. S.; Keene, F. R. *Chem.—Eur. J.* **2006**, *12*, 4873. (k) D'Alessandro, D. M.; Keene, F. R. *New J. Chem.* **2006**, *30*, 228. (l) Maji, S.; Sarkar, B.; Mobin, S. M.; Fiedler, J.; Kaim, W.; Lahiri, G. K. *Dalton Trans.* **2007**, 2411. (m) Loiseau, F.; Nastasi, F.; Stadler, A.-M.; Campagna, S.; Lehn, J.-M. *Angew. Chem., Int. Ed.* **2007**, *46*, 6144. (n) Stagni, S.; Orselli, E.; Palazzi, A.; Cola, L. D.; Zacchini, S.; Femoni, C.; Marcaccio, M.; Paolucci, F.; Zanarini, S. *Inorg. Chem.* **2007**, *46*, 9126. (o) Govindaswamy, P.; Therrien, B.; Süss-Fink, G.; Štěpnička, P.; Ludvík, J. *J. Organomet. Chem.* **2007**, *692*, 1661. (p) Ghumaan, S.; Sarkar, B.; Patil, M. P.; Fiedler, J.; Sunoj, R. B.; Kaim, W.; Lahiri, G. K. *Polyhedron* **2007**, *26*, 3409. (q) Therrien, B.; Süss-Fink, G.; Govindaswamy, P.; Saïd-Mohamed, C. *Polyhedron* **2007**, *26*, 4065. (r) Herrera, J.-M.; Pope, S. J. A.; Meijer, A. J. H. M.; Easun, T. L.; Adams, H.; Alsindi, W. Z.; Sun, X.-Z.; George, M. W.; Faulkner, S.; Ward, M. D. *J. Am. Chem. Soc.* **2007**, *129*, 11491. (s) Xun, S.; Zhang, J.; Li, X.; Ma, D.; Wang, Z. Y. *Synth. Met.* **2008**, *158*, 484. (t) Salsman, J. C.; Kubiak, C. P.; Ito, T. *J. Am. Chem. Soc.* **2005**, *127*, 2382. (u) Londergan, C. H.; Salsman, J. C.; Lear, B. J.; Kubiak, C. P. *Chem. Phys.* **2006**, *324*, 57.

(4) (a) Hush, N. S. *Prog. Inorg. Chem.* **1967**, *8*, 391. (b) Hush, N. S. *Coord. Chem. Rev.* **1985**, *64*, 135. (c) Creutz, C.; Newton, M. D.; Sutin, N. *J. Photochem. Photobiol. A* **1994**, *82*, 47.

(5) (a) Petrov, V.; Hupp, J. T.; Mottley, C.; Mann, L. C. *J. Am. Chem. Soc.* **1994**, *116*, 2171. (b) Oh, D. H.; Sano, M.; Boxer, S. G. *J. Am. Chem. Soc.* **1991**, *113*, 6880. (c) Rocha, R. C.; Brown, M. G.; Londergan, C. H.; Salsman, J. C.; Kubiak, C. P.; Shreve, A. P. *J. Phys. Chem. A* **2005**, *109*, 9006.

(6) (a) Prassides, K, Ed. *Mixed Valency Systems—Applications in Chemistry, Physics and Biology*; Kluwer Academic Publishers: Dordrecht, The Netherlands, 1991. (b) Fabre, M.; Bonvoisin, J. *J. Am. Chem. Soc.* **2007**, *129*, 1434. (c) Richardson, D. E.; Taube, H. *Coord. Chem. Rev.* **1984**, *60*, 107. (d) Crutchley, R. J. *Adv. Inorg. Chem.* **1994**, *41*, 273. (e) Demadis, K. D.; Hartshorn, D. C.; Meyer, T. J. *Chem. Rev.* **2001**, *101*, 2655.

(7) (a) Braun-Sand, S. B.; Wiest, O. *J. Phys. Chem. B* **2003**, *107*, 9624. (b) Braun-Sand, S. B.; Wiest, O. *J. Phys. Chem. A* **2003**, *107*, 285. (c) Wang, Y.; Lieberman, M. *IEEE Trans. Nanotech.* **2004**, *3*, 368. (d) Zhao, P.; Woolard, D.; Seminario, J. M.; Trew, R. *Int. J. High Speed Electron.* **2006**, *16*, 705. (e) Lent, C. S.; Isaksen, B.; Lieberman, M. *J. Am. Chem. Soc.* **2003**, *125*, 1056.

(8) (a) Baumann, J. A.; Meyer, T. J. *Inorg. Chem.* **1980**, *19*, 345. (b) Heyduk, A. F.; Nocera, D. G. *Science* **2001**, *293*, 1639.

(9) Kaim, W. *Angew. Chem.* **1983**, *95*, 201. *Angew. Chem., Int. Ed. Engl.* **1983**, *22*, 171.

(10) (a) Ruminski, R.; Kiplinger, J.; Cockroft, T.; Chase, C. *Inorg. Chem.* **1989**, *28*, 370. (b) Collin, J.-P.; Laine, P.; Launay, J.-P.; Sauvagea, J.-P.; Soura, A. *J. Chem. Soc., Chem. Commun.* **1993**, 434. (c) Arana, C. R.; Abruna, H. D. *Inorg. Chem.* **1993**, *32*, 194. (d) Jones, S. W.; Vrana, L. M.; Brewer, K. J. *J. Organomet. Chem.* **1998**, *554*, 29. (e) Haga, M.; Kato, N.; Monjushiro, H.; Wang, K.; Hossain, Md. D. *Supramol. Sci.* **1998**, *5*, 337. (f) Hartshorn, V.; Daire, N.; Tondreau, V.; Loeb, B.; Meyer, T. J.; White, P. S. *Inorg. Chem.* **1999**, *38*, 3200. (g) Chanda, N.; Laye, R. H.; Chakraborty, S.; Paul, R. L.; Jeffery, J. C.; Ward, M. D.; Lahiri, G. K. *J. Chem. Soc., Dalton Trans.* **2002**, 3496. (h) Chanda, N.; Sarkar, B.; Fiedler, J.; Kaim, W.; Lahiri, G. K. *Dalton Trans.* **2003**, 3550. (i) Chanda, N.; Sarkar, B.; Kar, S.; Fiedler, J.; Kaim, W.; Lahiri, G. K. *Inorg. Chem.* **2004**, *43*, 5128. (j) Ghumaan, S.; Sarkar, B.; Chanda, N.; Sieger, M.; Fiedler, J.; Kaim, W.; Lahiri, G. K. *Inorg. Chem.* **2006**, *45*, 7955. (k) Koley, M.; Sarkar, B.; Ghumaan, S.; Bulak, E.; Fiedler, J.; Kaim, W.; Lahiri, G. K. *Inorg. Chem.* **2007**, *46*, 3736. (l) Kaim, W.; Lahiri, G. K. *Angew. Chem., Int. Ed.* **2007**, *46*, 1778. (m) Rocha, R. C.; Rein, F. N.; Jude, H.; Shreve, A. P.; Concepcion, J. J.; Meyer, T. J. *Angew. Chem., Int. Ed.* **2008**, *47*, 503. (n) Das, A. K.; Sarkar, B.; Fiedler, J.; Záliš, S.; Hartenbach, I.; Strobel, S.; Lahiri, G. K.; Kaim, W. *J. Am. Chem. Soc.* **2009**, *131*, 8895. (o) Wadman, S. H.; Havenith, R. W. A.; Hartl, F.; Lutz, M.; Spek, A. L.; van Klink, G. P. M.; van Koten, G. *Inorg. Chem.* **2009**, *48*, 5685. (p) Bernhard, S.; Takada, K.; Díaz, D. J.; Abruña, H. D.; Mürne, H. *J. Am. Chem. Soc.* **2001**, *123*, 10265. (q) Fantacci, S.; Angelis, F. D.; Wang, J.; Bernhard, S.; Selloni, A. *J. Am. Chem. Soc.* **2004**, *126*, 9715.

(11) (a) Zhou, P.; O'Hagan, D.; Mocek, U.; Zeng, Z.; Yuen, L. D.; Frenzel, T.; Unkefer, C. J.; Beale, J. M.; Floss, H. G. *J. Am. Chem. Soc.* **1989**, *111*, 7274. (b) Kottwitz, K.; Laschinsky, N.; Fischer, R.; Nielsen, P. *Biometals* **2009**, *22*, 289.

Scheme 1. Possible Isomeric Forms of **1**−**3**

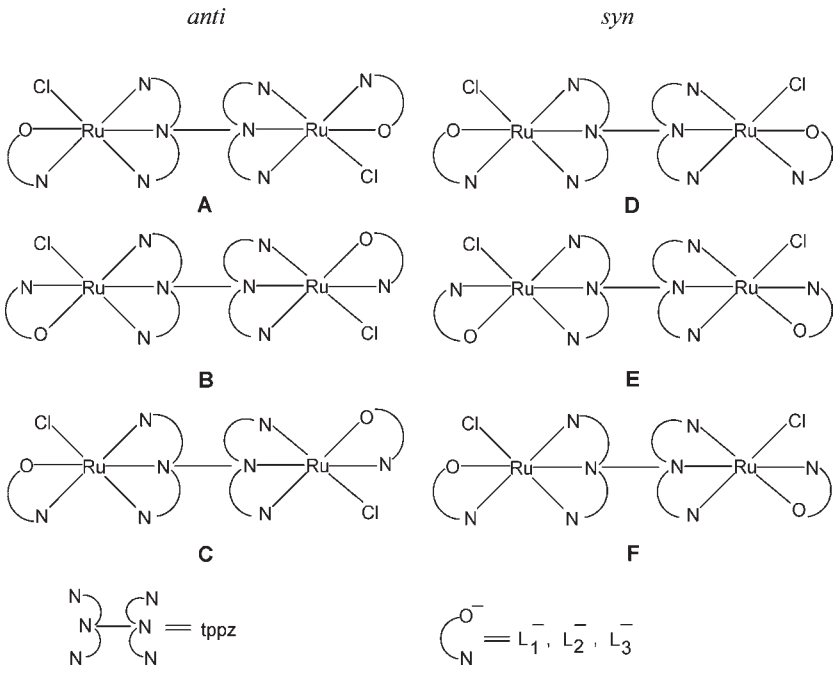

Results and Discussion

Synthesis and Identification. The tppz-bridged dinuclear complexes $[\{Ru^{II}(L_{1-3})Cl\}_2(\mu\text{-tppz})]$ (**1**−**3**) have been synthesized via reactions of the precursor complex $[(Cl_3Ru^{III})_2(\mu\text{-tppz})]$ with the respective protonated forms HL_{1-3} of the ALs (see the Experimental Section). The dinuclear complexes **1**−**3** can exist in six isomeric forms (idealized formulas **A**−**F**, Scheme 1) considering (i) the alternative mutual disposition of the two Ru−Cl groups, anti (**A**−**C**) or syn (**D**−**F**), and (ii) the relative orientations of the N,O^- donors of the two asymmetric chelate ligands L^-. The nonplanar configuration of coordinated tppz caused by interfering C−H bonds was established earlier,[10f,g,m,n] leading to deviations from the idealized description.

In all three cases **1**−**3**, only one isomer has been observed by NMR and isolated. The crystal structure determinations of **1**−**3** authenticate their isomeric identities as **B**, **D**, and **B**, respectively (Scheme 1, see later). The arrangement of largely syn-oriented Ru−Cl groups as in **2** was reported earlier in the crystal structure of the analogous complex $[(bpy')(Cl)Ru^{II}(\mu\text{-tppz})Ru^{II}(Cl)(bpy')](PF_6)_2$ (bpy′ = 4,4′-dimethyl-2,2′-bipyridine),[10f] which was isolated as a minor product along with the corresponding anti isomer as a major constituent. In contrast, the crystal structures of two other such complexes, $[(pap)ClRu^{II}(\mu\text{-tppz})Ru^{II}Cl(pap)](ClO_4)_2$ (pap = 2-phenylazopyridine)[10g] and $[(Q)(Cl)Ru^{II}(\mu\text{-tppz})Ru^{II}(Cl)(Q)](PF_6)_2$ (Q = 4,6-di-*tert*-butyl-*N*-phenyl-*o*-iminobenzosemiquinonato),[10n] exhibited an approximately anti orientation of the two Ru−Cl bonds like in **1** and **3**.

The diamagnetic and nonconducting compounds **1**−**3** exhibit satisfactory microanalytical (C, H, and N) and mass spectral data (Figure S1 in the SI). The ν(C═O) frequencies of the free ligands (HL_1−HL_3) near 1700 cm^{-1} are decreased to about 1600 cm^{-1} upon coordination in **1**−**3**. The ^1H NMR spectra in $(CD_3)_2SO$ show 12 and 14 proton signals for **1** and **3**, respectively, as expected for centrosymmetric anti-isomeric form **B**, whereas **2** exhibits 28 proton resonances because of its syn geometry **D** (see the Experimental Section).

Crystal Structures. The crystal structures establish that complexes **1** (its asymmetric unit contains two molecules, **1a** and **1b**) and **3** were obtained in an approximately anti form (Figures 1 and 3 and S2 and S3a,c in the SI and Tables 1 and 2 and S1−S4 in the SI), whereas **2** approaches the syn configuration (Figures 2 and S3b in the SI). Accordingly, the ClRuRu′Cl′ angles are 149.86° (**1a**), 153.72° (**1b**), 32.54° (**2**), and 138.81° (**3**).

The structural features of the isomeric quinolinecarboxylato ALs L_2^- and L_3^- in **2** and **3** lead to the following differences: (i) The Ru−Cl groups adopt syn and anti configurations in **2** and **3**, respectively, (ii) the quinaldate L_2^- forms five-membered chelate rings, while L_3^- causes six-membered ring chelate formation, and (iii) the N,O^- donors of the asymmetric chelate ligands L_2^- and L_3^- bind to the metal ions differently. The O donors of two L_2^- ligands in **2** and the N donors of two L_3^- ligands in **3** are trans to the pyrazine N atom of μ-tppz, yielding the **B** and **D** structural forms, respectively, from Scheme 1. The difference in the geometry between **1** and **2**, anti and syn, depending on one additional fused benzo ring, is rather surprising. The RuN_4OCl coordination arrangement

(12) (a) Warren, S.; McCormac, T.; Dempsey, E. *Bioelectrochemistry* **2005**, *67*, 23. (b) Saburi, H.; Tanaka, S.; Kitamura, M. *Angew. Chem., Int. Ed.* **2005**, *44*, 1730. (c) Zhang, H.-J.; Demerseman, B.; Toupet, L.; Xi, Z.; Bruneau, C. *Adv. Synth. Catal.* **2008**, *350*, 1601.

(13) (a) Canty, A. J.; Traill, P. R.; Skelton, B. W.; White, A. H. *Inorg. Chim. Acta* **1997**, *255*, 117. (b) Sengupta, P.; Dinda, R.; Ghosh, S.; Sheldrick, W. S. *Polyhedron* **2001**, *20*, 3349. (c) Rachford, A. A.; Petersen, J. L.; Rack, J. J. *Dalton Trans.* **2007**, 3245. (d) Fukui, S.; Shimamura, Y.; Sunamoto, Y.; Abe, T.; Hirano, T.; Oi, T.; Nagao, H. *Polyhedron* **2007**, *26*, 4645. (e) Matsumura, S.; Shikano, K.; Oi, T.; Suzuki, N.; Nagao, H. *Inorg. Chem.* **2008**, *47*, 9125.

(14) (a) Zhang, H.-J.; Demerseman, B.; Toupet, L.; Xi, Z.; Bruneau, C. *Organometallics* **2009**, *28*, 5173. (b) Małecki, J. G.; Kruszyński, R.; Tabak, D.; Kusz, J. *Polyhedron* **2007**, *26*, 5120. (c) Halpenny, G. M.; Mascharak, P. K. *Inorg. Chem.* **2009**, *48*, 1490.

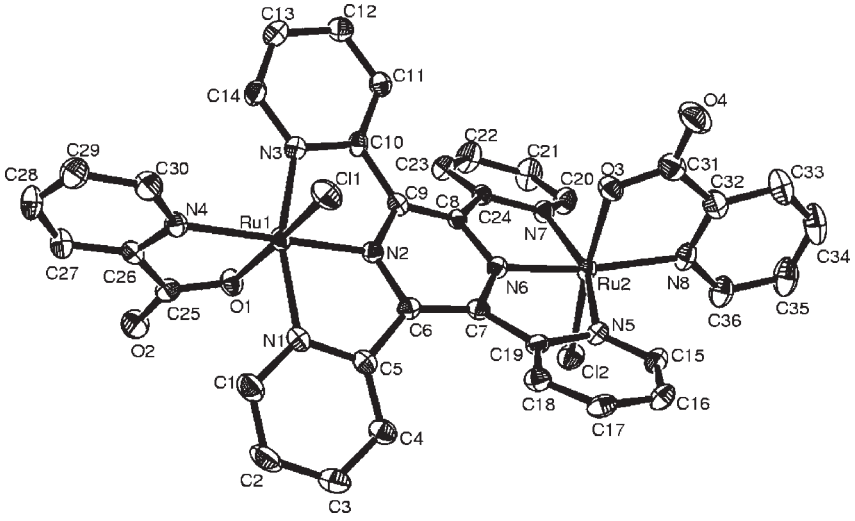

Figure 1. ORTEP diagram of molecule **1a** from the crystal. Ellipsoids are drawn at the 50% probability level. Solvents of crystallization are removed for clarity.

Table 1. Crystallographic Data for **1**−**3**

	1	**2**	**3**
formula	$C_{74}H_{57}Cl_4N_{17}O_{11}Ru_4$	$C_{51}H_{28}Cl_2N_8O_8Ru_2$	$C_{50}H_{28}Cl_2N_8O_4Ru_2$
fw	1906.45	1153.85	1077.84
cryst size (mm)	0.28 × 0.24 × 0.21	0.33 × 0.26 × 0.21	0.28 × 0.24 × 0.22
radiation	Mo Kα	Mo Kα	Mo Kα
cryst syst	monoclinic	monoclinic	monoclinic
space group	$P2_1/n$	$P2_1/c$	$C2/c$
a (Å)	15.4120(2)	10.9787(11)	23.9051(8)
b (Å)	21.4214(3)	15.8256(14)	14.1541(5)
c (Å)	22.6136(3)	27.455(3)	13.3293(6)
β (deg)	104.5080(10)	98.031(10)	115.491(5)
V (Å^3)	7227.74(17)	4723.4(8)	4071.0(3)
Z	4	4	4
F(000)	3808	2304	2152
μ (mm^{-1})	1.043	0.818	0.935
T (K)	150(2)	150(2)	150(2)
hkl ranges	−22 to +23, −24 to +32, −33 to +32	−13 to +12, −18 to +18, −29 to +32	−28 to +28, −16 to +16, −15 to +15
ρ_{calcd} (g cm^{-3})	1.752	1.623	1.759
θ range (deg)	3.24−32.80	2.98−25.00	3.34−25.00
reflns collected	84 198	38 445	15 258
unique reflns (R_{int})	24 438 (0.0552)	8297 (0.1055)	3570 (0.0829)
data/restraints/param	24 438/0/1014	8297/10/605	3570/0/298
R1 [$I > 2\sigma(I)$]	0.0332	0.0769	0.0481
wR2 (all data)	0.0583	0.2102	0.0794
GOF	0.781	1.068	0.951
residual electron density: max, min (e Å^{-3})	0.703, −0.850	1.078, −0.969	0.792, −0.745

Table 2. Selected Bond Lengths [Å] for **1a**, **2**, and **3** in the Crystals[a]

		2		**3**	
bond length	**1a**	X-ray	DFT	X-ray	DFT
Ru1−N2	1.929(2)	1.904(8)	1.934	1.937(4)	1.958
Ru1−N1	2.036(2)	2.039(9)	2.067	2.046(4)	2.069
Ru1−N3	2.056(2)	2.044(9)	2.057	2.054(4)	2.076
Ru1−O1	2.073(2)	2.076(8)	2.089	2.060(4)	2.058
Ru1−N4	2.080(2)	2.107(9)	2.149	2.107(4)	2.145
Ru1−Cl1	2.3822(7)	2.365(3)	2.415	2.3728(14)	2.424
Ru2−N6	1.919(2)	1.899(9)	1.933		
Ru2−N5	2.031(2)	2.037(11)	2.057		
Ru2−N7	2.037(2)	2.030(8)	2.066		
Ru2−O3	2.056(2)	2.075(9)	2.090		
Ru2−N8	2.089(2)	2.081(10)	2.147		
Ru2−Cl2	2.3584(7)	2.377(3)	2.415		

[a] Data for molecule **1b** and selected bond angles are given in the SI.

around each Ru ion in **1**−**3** is distorted octahedral, as is evident even from the trans angles of about 160° associated with the meridionally coordinated tppz ligand. The cross-bridge Ru---Ru and Cl---Cl separations in **1**−**3** are 6.526/8.229 (**1a**), 6.563/8.087 (**1b**), 6.492/5.710 (**2**), and 6.530/7.408 Å (**3**). The Ru---Ru distances in **1**−**3** are comparable with those of the reported structurally characterized analogous complexes.[10f,g,n] The Cl---Cl distances in molecules **1a** and **1b** (> 8.0 Å) are appreciably longer than that in the other anti complex **3** at 7.408 Å or than the 5.710 Å in the largely syn-configured compound **2**. The reason for this lies in the more pronounced anti arrangement of **1a** and **1b** with ClRuRu′Cl′ angles of 149.86° and 153.72° versus 138.81° for **3** (Figure S3a,c in the SI), a consequence of the different chelate ring sizes. In the syn complex **2**, the two Ru−Cl groups also deviate substantially from coplanarity with an

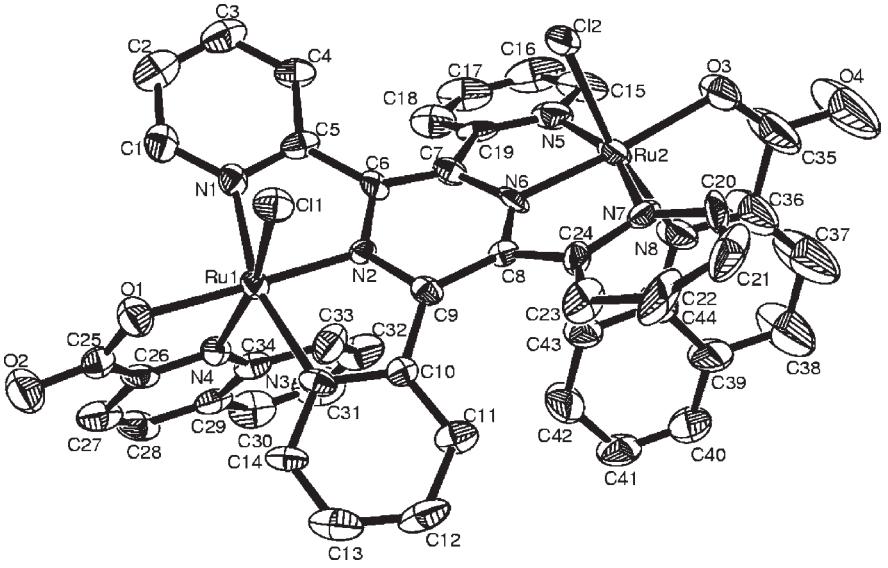

Figure 2. ORTEP diagram of **2** from the crystal. Ellipsoids are drawn at the 50% probability level. Solvents of crystallization are removed for clarity.

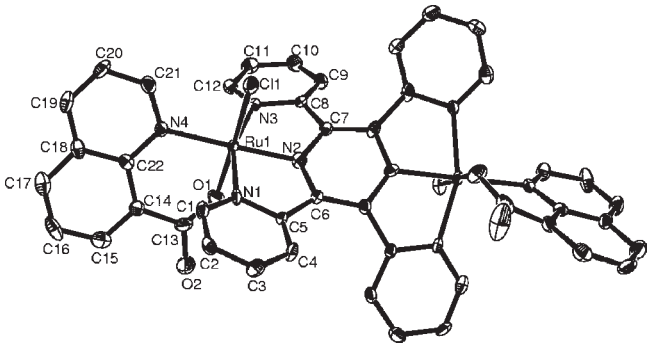

Figure 3. ORTEP diagram of **3** from the crystal. Ellipsoids are drawn at the 50% probability level. Solvent of crystallization is removed for clarity.

angle Ru1Cl1Ru2/Ru2Cl2Ru1 of 32.54° (Figure S3b in the SI).

The crystal structures of **1**−**3** reveal the nonplanarity of the bridging tppz ligand,[10f,g,m,n] which contains the pyridyl groups alternately displaced upward and downward around the central, considerably twisted (Figure S4 in the SI) pyrazine ring of tppz. The torsion angles between the adjacent pyridine rings in **1**−**3** are 31.62, 28.18° (**1a**), 24.39, 25.42° (**1b**), 26.42, 31.79° (**2**), and 30.60, 38.29° (**3**). The dihedral angle between the planes Ru1N1N2N3 and Ru2N5N6N7 in **2** is 33.66°. The central pyrazine rings of the coordinated tppz in **1**−**3** exhibit a distinct twist-boat conformation (Figure S4 in the SI) despite the aromatic character.

The distorted nonplanar situation of the bridging tppz ligand in **1**−**3** (Figures 1−3 and S2−S4 in the SI) has been confirmed by DFT-optimized structures of the representatives **2** and **3** (Figure S5 in the SI).

The shorter Ru−N(pyrazine,tppz) distances in **1**−**3** between 1.899(9) and 1.937(4) Å, as compared to the Ru−N(pyridine,tppz) distances ranging from 2.030(2) to 2.056(2) Å (Tables 2 and S4 in the SI), reflect the steric constraints of *mer*-tridentate coordination and imply strong $(d\pi)Ru^{II} \rightarrow (p\pi^*)$pyrazine(tppz) back-donation, which facilitates the bridge-mediated intermetallic electronic interaction in the mixed-valent $Ru^{III}Ru^{II}$ state via the electron-exchange pathway.[6d,10l] Further, the Ru−N(pyrazine,tppz) distances in the complexes are shorter than those at about 1.952(6) Å of the analogous complexes with AL = bpy[10f] or 2-phenylazopyridine.[10g] Apparently, the donor effect of L_{1-3} facilitates stronger pyrazine-mediated intermetallic coupling in the mixed-valent forms (see below).

The Ru−N and Ru−O bond distances associated with the $\{Ru-L_1\}$ and $\{Ru-L_2\}$ complex fragments in **1** and **2** are comparable with those in related structurally characterized compounds of ruthenium involving L_1^-[13] and L_2^-.[14] However, to the best of our knowledge, no ruthenium complex of L_3^- has been reported so far.

The hydrogen-bonding interactions in the crystals of **1** and **2** are given in Figures S6 and S7 and Tables S5 and S6 in the SI.

Electrochemistry and Spectroelectrochemistry. The dinuclear complexes **1**−**3** exhibit two successive reversible one-electron-oxidation and -reduction processes in CH_3CN (Figure 4 and Table 3). Starting from the diruthenium(II) valence configuration in the native states of **1**−**3**, the successive reversible one-electron-oxidation processes are assigned to the transitions $Ru^{II}Ru^{II} \rightleftharpoons Ru^{II}Ru^{III} \rightleftharpoons Ru^{III}Ru^{III}$.[15,10f−k] DFT calculations for the optimized structures of the representative compounds **2** and **3** (Figure S5 in the SI) also suggest that the highest occupied molecular orbital (HOMO) and singly occupied molecular orbital (SOMO) in **2**/**3** and $\mathbf{2}^+/\mathbf{3}^+$, respectively, are dominated by the Ru ions along with variable partial involvements from the other three ligand constituents, Cl, tppz, and L_2^- or L_3^- (Tables S7, S10, S8, and S11 in the SI). The first $Ru^{III}Ru^{II}$ oxidation potential varies slightly depending on the configuration, following the order **3** ≈ **1** < **2** (Table 3). The higher stability of the Ru^{II} state in **2** with respect to **1** can be attributed to the presence of the electron-withdrawing phenyl rings fused with the picolinate group. The higher stability of the Ru^{III} state in **3** (Table 3) can be interpreted in terms of the six-membered chelate ring in the framework of coordinated L_3^- in **3** against the five-membered chelate rings in **1** and **2**. In L_3^-, the donor centers (N, O) are spread over the two fused aromatic rings, while the donor centers of L_1^- and L_2^- in

(15) Patra, S.; Sarkar, B.; Ghumaan, S.; Fiedler, J.; Kaim, W.; Lahiri, G. K. *Inorg. Chem.* **2004**, *43*, 6108.

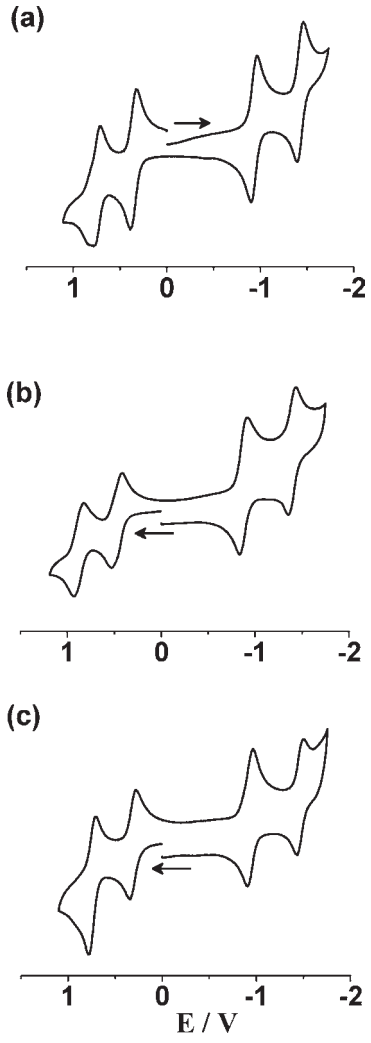

Figure 4. Cyclic voltammograms of (a) **1**, (b) **2**, and (c) **3** in CH_3CN/0.1 M NEt_4ClO_4 at 298 K. Scan rate: 100 mV s^{-1}.

1 and **2**, respectively, are part of the same ring. The closeness of the first $Ru^{III}Ru^{II}$ redox potentials for **1** and **3** is associated with their anti configuration (**B**, Scheme 1); their potential is 100 mV lower when compared to that of the syn-configured complex **2** (Table 3). The syn and anti isomers of the analogous AL = bpy ions $[(bpy)ClRu(\mu\text{-tppz})RuCl(bpy)]^{2+}$ failed to show any difference in their first $Ru^{III}Ru^{II}$ potentials.[10f]

There are just minor differences for **1**−**3** regarding their K_c (comproportionation constant[16]) values of $\sim 10^6-10^7$ (Table 3) for the $Ru^{III}Ru^{II}$ state. The K_c value of $> 10^6$ for **1**−**3** suggests a valence-delocalized (class III) mixed-valence situation according to the Robin and Day definition.[17] The K_c value of $> 10^6$ for **1**−**3** is comparable to that observed for the analogous complex with AL = 2,2′-dipyridylamine.[10h] Other tppz-bridged frameworks {(AL)Ru(μ-tppz)Ru(AL)} with different pyridine- or imidazole-based acceptor ALs (Scheme S1 in the SI) exhibit lower K_c values in the order of 10^3-10^4 because the parallel $Ru^{II} \rightarrow (\pi^*)$AL back-donation to the π-acceptor ALs decreases the π^*-tppz-mediated valence exchange efficiency between the metal termini in the mixed-valent {(AL)Ru^{II}(μ-tppz)Ru^{III}(AL)} state.[10f,g,i−k]

Table 3. Electrochemical Data[a]

	E°_{298} [V] (ΔE_p [mV]) [b]					
complex	ox 1	ox 2	red 1	red 2	K_{c1} [c,d]	K_{c2} [c,e]
1	0.36 (66)	0.75 (73)	−0.93 (58)	−1.43 (65)	4×10^6	2.9×10^8
2	0.47 (109)	0.88 (94)	−0.87 (79)	−1.39 (73)	8.9×10^6	6.5×10^8
3	0.31 (69)	0.74 (78)	−0.93 (63)	−1.46 (70)	1.9×10^7	9.6×10^8

[a] From cyclic voltammetry in CH_3CN/0.1 M Et_4NClO_4 at 100 mV s^{-1}. [b] In V vs SCE; peak potential differences ΔE_{pp} [mV] (in parentheses). [c] Comproportionation constant from $RT \ln K_c = nF(\Delta E)$. [d] K_{c1} between ox 1 and ox 2. [e] K_{c2} between red 1 and red 2.

DFT calculations suggest that the lowest unoccupied molecular orbitals (LUMOs) or SOMOs in the optimized species **2**, **3** and $\mathbf{2}^-$, $\mathbf{3}^-$ (β spin), respectively, should be dominated by the tppz-based π^* orbitals (Tables S7, S10 and S9, S12 in the SI). The two successive reduction processes (Figure 4 and Table 3) in **1**−**3** are therefore assigned to the stepwise tppz-based reductions, tppz $\rightleftharpoons$ $tppz^{\bullet-} \rightleftharpoons tppz^{2-}$.[10] The involvement of L-based molecular orbitals in the LUMO (α spin) and LUMO+1 (β spin) of $\mathbf{2}^-$ and $\mathbf{3}^-$ (Tables S9 and S12 in the SI) suggests the possibility of subsequent reduction(s) of the ALs; however, no such reductions have been detected experimentally within the redox potential limit of −2.0 V vs SCE in CH_3CN. The separation of potentials between the successive two-step tppz reductions leads to an invariant K_c value in the range of 10^8-10^9 (Table 3), implying the stability of the intermediate radical state $[(L_{1-3}^-)ClRu^{II}(\mu\text{-tppz}^{\bullet-})Ru^{II}Cl(L_{1-3}^-)]^{\bullet-}$ on the time scale of cyclic voltammetry.[10]

The complexes **1**−**3** exhibit intense ligand-based transitions in the UV region and multiple, moderately strong transitions in the visible region between 1000 and 400 nm (Table 4 and Figures 5 and S8 and S9 in the SI). The lowest-energy transitions for the anti-configured complexes **1** and **3** appear at positions of 980 and 990 nm, respectively, which are close by, whereas a similar transition in the syn-configured complex **2** takes place at higher energy, at 905 nm (Table 4), implying a greater HOMO−LUMO energy separation in **2**, as has been reflected by the redox potentials (Table 3). Moreover, DFT calculations also predict a larger HOMO−LUMO energy separation for **2** (1.97 eV) as compared to **3** (1.88 eV; Figure 6). The bands in the regions 900−1000, 600−700, and 470−480 nm in **1**−**3** are assigned on the basis of TD-DFT calculations for optimized structures of **2** and **3** as metal (dπ)-to-ligand (π^*-tppz) charge-transfer (MLCT), metal−ligand ($L^-/Cl^-(p\pi)$)-to-ligand (π^*-tppz) charge-transfer (MLLCT), and ligand-to-ligand charge-transfer, L^- to π^*-tppz (LLCT)/ligand ($Cl^-(p\pi)$)−metal-to-ligand ($L^-(\pi^*)$) charge-transfer (LMLCT) transitions, respectively (Tables 4 and S13 and S14 in the SI and Figures 5 and S8 and S9 in the SI).

Upon one-electron oxidation to the $Ru^{III}Ru^{II}$ mixed-valent state in $\mathbf{1}^+-\mathbf{3}^+$, the MLCT and MLLCT bands are blue-shifted with a reduction in intensity, in corroboration with a decrease from two Ru^{II} centers in **1**−**3** to only one Ru^{II} site in $\mathbf{1}^+-\mathbf{3}^+$ (Figures 5 and S8 and S9 in the SI and Tables 4 and S13 and S14 in the SI).[18] The mixed-valent

(16) Creutz, C. *Prog. Inorg. Chem.* **1983**, *30*, 1.
(17) Robin, M. B.; Day, P. *Adv. Inorg. Radiochem.* **1967**, *10*, 247.

Table 4. UV/Vis/Near-IR Spectroelectrochemical Data for **1**−**3** in CH_3CN/0.1 M Bu_4NPF_6

complex	λ_{max} [nm] (ε [M^{-1} cm^{-1}])
$\mathbf{1}^{2+}$	480 (8400), 386 (36 400), 368 (sh), 298 (26 200), 264 (28 900), 240 (28 800)
$\mathbf{1}^{+}$	1670 (2600, 1615 cm^{-1}), 920 (sh), 618 (16 100), 366 (32 000), 297 (27 000), 252 (28 400), 220 (21 300)
1	980 (2300), 651 (24 500), 480 (7500), 430 (sh), 360 (38 000), 297 (26 000), 256 (31 100), 221 (21 200)
$\mathbf{1}^{-}$	1215 (5800), 995 (4300), 920 (4100), 760 (sh), 634 (13 700), 570 (sh), 485 (sh), 435 (32 900), 392 (32 800), 373 (sh), 319 (24 000), 257 (28 800), 217 (24 800)
$\mathbf{1}^{2-}$	1670 (450), 1135 (8400), 995 (5500), 785 (sh), 710 (sh), 663 (15 700), 565 (sh), 466 (33 400), 376 (38 700), 300 (sh), 258 (28 200), 218 (28 000)
$\mathbf{2}^{2+}$	570 (sh), 490 (6600), 391 (25 200), 372 (sh), 309 (20 300), 243 (24 500)
$\mathbf{2}^{+}$	1575 (1200, 1150 cm^{-1}), 890 (sh), 601 (11 200), 372 (22 200), 299 (21 500), 242 (24 500)
2	905 (2000), 642 (17 300), 460 (9700), 361 (24 000), 300 (24 200), 242 (25 800)
$\mathbf{2}^{-}$	1192 (3700), 990 (sh), 902 (3300), 629 (11 100), 500 (sh), 433 (18 600), 388 (20 200), 306 (23 400), 240 (32 700)
$\mathbf{3}^{2+}$	553 (5800), 473 (sh), 390 (28 100), 371 (25 400), 305 (24 700), 238 (28 700)
$\mathbf{3}^{+}$	1875 (2600, 1365 cm^{-1}), 955 (sh), 654 (12 800), 372 (26 000), 300 (25 000), 237 (29 400)
3	990 (2100), 695 (20 500), 470 (sh), 363 (27 500), 296 (27 300), 237 (29 900)
$\mathbf{3}^{-}$	1261 (4200), 1030 (sh), 930 (3700), 755 (sh), 676 (12 000), 590 (sh), 490 (sh), 441 (22 200), 393 (22 200), 300 (26 200), 235 (31 500)

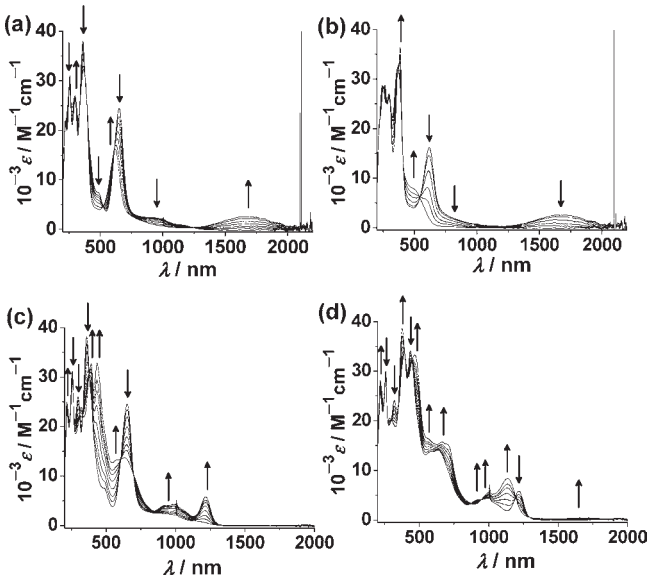

Figure 5. UV/vis/near-IR spectroelectrochemistry for the conversions of (a) $\mathbf{1}\rightarrow\mathbf{1}^{+}$, (b) $\mathbf{1}^{+}\rightarrow\mathbf{1}^{2+}$, (c) $\mathbf{1}\rightarrow\mathbf{1}^{-}$, and (d) $\mathbf{1}^{-}\rightarrow\mathbf{1}^{2-}$ in CH_3CN/0.1 M Bu_4NPF_6.

species $\mathbf{1}^{+}$−$\mathbf{3}^{+}$ exhibit moderately intense $Ru^{II}\rightarrow Ru^{III}$ intervalence charge-transfer (IVCT) absorption maxima in the range of 1500−1900 nm.[10] Remarkably, the positions as well as the intensities of the IVCT bands vary distinctly in $\mathbf{1}^{+}$−$\mathbf{3}^{+}$, depending on the structural/electronic features of the ALs and overall structural features like anti/syn isomerism (Figures 5 and S8 and S9 in the SI and Tables 4 and S13 and S14 in the SI). The energy of the IVCT band for the syn-configured complex **2** (1575 nm, 6350 cm^{-1}; ε = 1200 M^{-1} cm^{-1}) is about 1000 cm^{-1} higher, and the band is less intense in comparison to that of the isomeric anti-configured complex **3** (1875 nm, 5330 cm^{-1}; ε = 2600 M^{-1} cm^{-1}). Accordingly, the TD-DFT calculations on the optimized $\mathbf{2}^{+}$ and $\mathbf{3}^{+}$ structures also suggest moderately intense Ru(dπ) → Ru(dπ) [HOMO(β) → LUMO(β)] IVCT transitions at 1459 nm [ε = 1933 $M^{-1}cm^{-1}$; experimental data 1575 nm (ε = 1200 M^{-1} cm^{-1})] for $\mathbf{2}^{+}$ and 1826 nm [ε = 4520 $M^{-1}cm^{-1}$; experimental data 1875 nm (ε = 2600 M^{-1} cm^{-1})] for $\mathbf{3}^{+}$

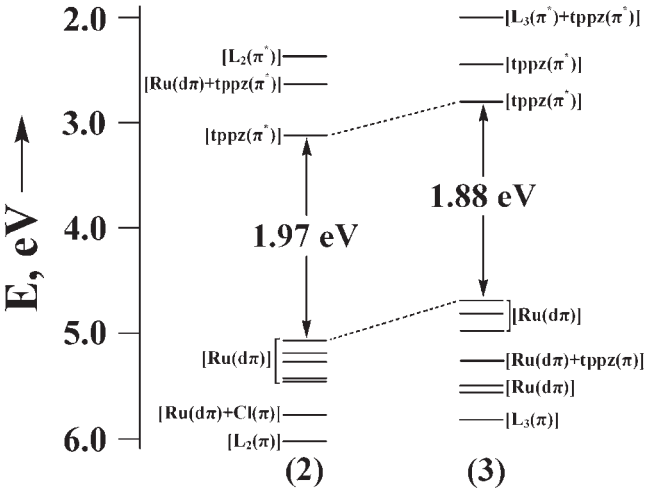

Figure 6. Orbital energy diagrams for isomeric **2** and **3**.

(Tables 4 and S13 and S14 in the SI and Figures S8 and S9 in the SI). The experimental bandwidths of the IVCT transitions in $\mathbf{1}^{+}$−$\mathbf{3}^{+}$ of 1620, 1150, and 1370 cm^{-1}, respectively (Table 4), are much smaller than those calculated as 3720, 3830, and 3510 cm^{-1}, respectively, using the Hush formula, $\Delta\nu_{1/2} = (2310E_{op})^{1/2}$ (E_{op} = energy of the IVCT band in cm^{-1})[4,7] for valence-localized class II mixed-valent states, implying a valence-averaged situation for $\mathbf{1}^{+}$−$\mathbf{3}^{+}$.

Upon further oxidation to the isovalent $Ru^{III}Ru^{III}$ forms $\mathbf{1}^{2+}$−$\mathbf{3}^{2+}$, the IVCT band expectedly disappears and the Ru^{II}-based MLCT/MLLCT absorptions get replaced by higher-energy Ru^{III} involving LMCT transitions near 500 nm (Table 4 and S13 and S14 in the SI and Figures 5 and S8 and S9 in the SI).

Although the IVCT absorptions[19] of $\mathbf{1}^{+}$−$\mathbf{3}^{+}$ correspond to $Ru^{III}Ru^{II}$ states, the paramagnetic intermediates failed to show any EPR signals in the X band, even at 4 K. Mixed-valent $Ru^{III}Ru^{II}$ situations without detectable EPR signals have also been found in other cases due to fast relaxation.[2,20] While EPR information could thus not be obtained experimentally, the spin-density plots of

(18) Sarkar, B.; Laye, R. H.; Mondal, B.; Chakraborty, S.; Paul, R. L.; Jeffery, J. C.; Puranik, V. G.; Ward, M. D.; Lahiri, G. K. *J. Chem. Soc., Dalton Trans.* **2002**, 2097.

(19) Sarkar, B.; Kaim, W.; Klein, A.; Schwederski, B.; Fiedler, J.; Duboc-Toia, C.; Lahiri, G. K. *Inorg. Chem.* **2003**, *42*, 6172.

(20) Maji, S.; Sarkar, B.; Mobin, S. M.; Fiedler, J.; Urbanos, F. A.; Jimenez-Aparicio, R.; Kaim, W.; Lahiri, G. K. *Inorg. Chem.* **2008**, *47*, 5204.

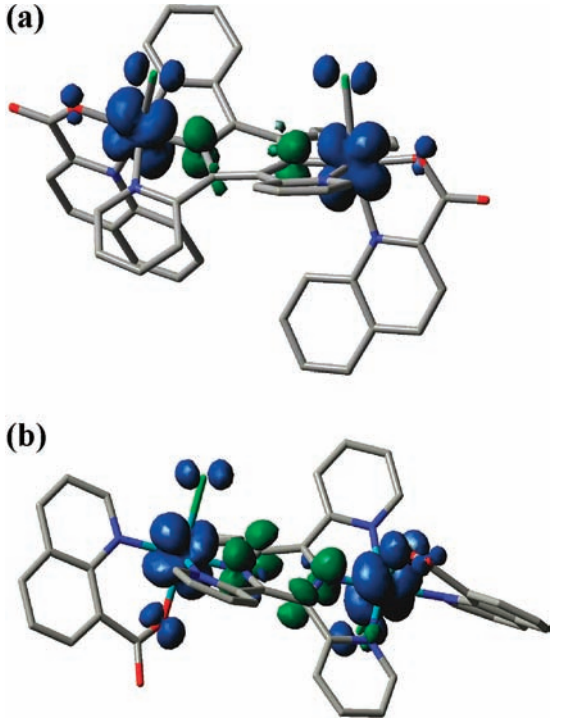

Figure 7. Spin-density plots of (a) $\mathbf{2}^{+}$ and (b) $\mathbf{3}^{+}$.

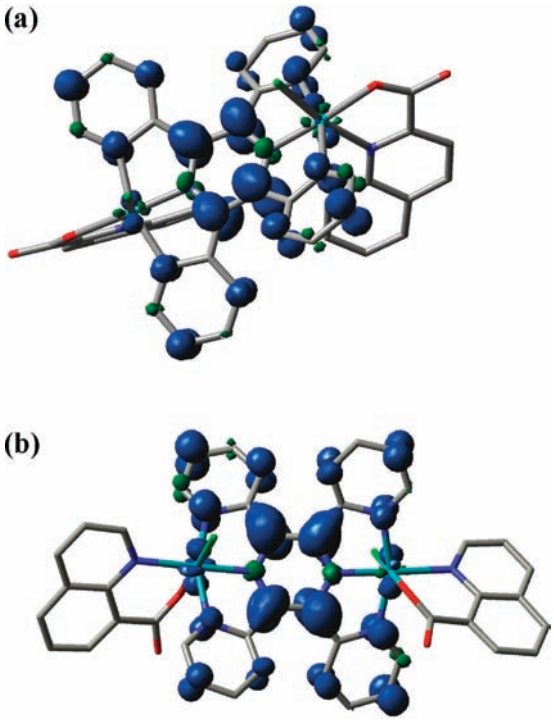

Figure 8. Spin-density plots of (a) $\mathbf{2}^{-}$ and (b) $\mathbf{3}^{-}$.

the mixed-valent $\mathbf{2}^{+}$ and $\mathbf{3}^{+}$ (Figure 7) show metal-centered calculated Mulliken spin densities of 0.605/0.584, 0.579/0.517, 0.118/0.082, 0.032/0.121, and −0.31/−0.295 on Ru1, Ru2, Cl, O, and tppz, respectively.

The spin-density plots of the one-electron-reduced states in $\mathbf{2}^{-}/\mathbf{3}^{-}$ show that the bridging tppz ligand is the spin-bearing center with Mulliken spin densities of 0.967/0.964 and 0.022/0.022 on tppz and Ru, respectively (Figure 8). Accordingly, the tppz-radical-bridged diruthenium(II) complexes $[(L_{1-3}^{-})Ru(\mu\text{-}tppz^{\bullet-})Ru(L_{1-3}^{-})]^{\bullet-}$ ($\mathbf{1}^{-}-\mathbf{3}^{-}$) exhibit organic radical-type EPR spectra at 110 K with slight metal contributions as predicted by the spin-density plots of $\mathbf{2}^{-}$ and $\mathbf{3}^{-}$ and as is evident from the small g factor anisotropy[21] ($\mathbf{1}^{-}$, $g_{\parallel}$, 2.0093, $g_{\perp}$, 1.9947; $\mathbf{2}^{-}$, $g_{\parallel}$, 2.010, $g_{\perp}$, 1.9947; $\mathbf{3}^{-}$, $g_{\parallel}$, 2.008, $g_{\perp}$, 1.996; Figure S10 in the SI).[10c−f] The anion-radical complexes $\mathbf{1}^{-}-\mathbf{3}^{-}$ exhibit a moderately intense near-IR absorption band in the range between 1100 and 1300 nm (Table 4 and Figures 5 and S8 and S9 in the SI), which is assigned to the known[10n] tppz-based intraligand $\pi \rightarrow \pi^{*}$ transition, as is also suggested by the TD-DFT calculations of $\mathbf{2}^{-}$ and $\mathbf{3}^{-}$ (Tables S13 and S14 in the SI).[10,22] The TD-DFT-calculated multiple $Ru^{II} \rightarrow$ tppz MLCT transitions for $\mathbf{2}^{-}$ and $\mathbf{3}^{-}$ (Tables S13 and S14 in the SI) appear in a similar region for all three complexes (Table 4 and Figures 5 and S8 and S9 in the SI).

Though the doubly reduced species $\mathbf{1}^{2-}-\mathbf{3}^{2-}$ are found to be formed reversibly on the cyclic voltammetric time scale used, the spectroelectrochemistry experiments at room temperature suggest a less reversible formation of $\mathbf{2}^{2-}$ and $\mathbf{3}^{2-}$. The reversible second reduction process in the case of $\mathbf{1}^{2-}$ reveals the presence of one weak transition in the near-IR region at 1670 nm (ε = 450 M^{-1} cm^{-1}) in addition to two moderately intense low-energy absorptions at 1135 nm (ε = 8400 M^{-1} cm^{-1}) and 995 nm (ε = 5500 M^{-1} cm^{-1}) (Figure 5 and Table 4), which are believed to be the intra/interligand transitions between $tppz^{2-}$ and unreduced ancillary (L^{-}) ligands.[23] The Ru^{II}-based intense MLCT transitions are also observed in the visible region (Figure 5 and Table 4).

Conclusion

Using an established[10] test system for intramolecular electron transfer, we could present three experimentally and computationally characterized complexes with rather different individual features:

a Compounds **1** and **3** share the anti configuration, while compound **2** was isolated in the syn form.

b Complexes **1** and **2** have five-membered chelate rings, while compound **3** features six-membered chelate rings.

c Compounds **2** and **3** are isomeric, involving quinolinecarboxylates as ALs.These different coordination situations notwithstanding, all complexes exhibit a considerably distorted tppz bridge with a twisted central pyrazine ring undergoing stepwise double one-electron reduction with a radical complex intermediate, as is evident from EPR and UV/vis spectroelectrochemistry. On the other hand, two well-separated ($\Delta E \sim 0.4$ V) one-electron oxidations occur on the metals to yield typically EPR-silent $Ru^{III}Ru^{II}$ intermediates with near-IR

(21) Kaim, W.; Ernst, S.; Kasack, V. *J. Am. Chem. Soc.* **1990**, *112*, 173.
(22) (a) Fletcher, N. C.; Robinson, T. C.; Behrendt, A.; Jeffery, J. C.; Reeves, Z. R.; Ward, M. D. *J. Chem. Soc., Dalton Trans.* **1999**, 2999. (b) Ghosh, A. K.; Peng, S.-M.; Paul, R. L.; Ward, M. D.; Goswami, S. *J. Chem. Soc., Dalton Trans.* **2001**, 336. (c) Auburn, P. R.; Lever, A. B. P. *Inorg. Chem.* **1990**, *29*, 2551. (d) Heath, G. A.; Yellowlees, L. J.; Braterman, P. S. *Chem. Phys. Lett.* **1982**, *92*, 646.
(23) Patra, S.; Sarkar, B.; Ghumaan, S.; Fiedler, J.; Záliš, S.; Kaim, W.; Lahiri, G. K. *Dalton Trans.* **2004**, 750.

absorption maxima between 1500 and 1900 nm. DFT/TD-DFT calculations confirm the experimental structures and also the subtle but notable differences in the otherwise rather invariant spectroscopic features of the [Ru(μ-tppz)Ru]^n entity, despite different coordination situations at the metal sites. This result relates to the necessary tolerance of useful multielectron redox-active components for, e.g., nanoparticle-adhesive carboxylate functions; it explains the previous success of this platform [Ru(μ-tppz)Ru]^n in extended systems[10p,q] and suggests its further use.

Experimental Section

General Procedures. The starting complex [Cl_3Ru^{III}(μ-tppz)$Ru^{III}Cl_3$] was prepared according to the reported procedure.[10f] The ligands 2-picolinic acid (HL_1), quinaldic acid (HL_2), and 8-quinolinecarboxylic acid (HL_3) were purchased from Aldrich, USA. Other chemicals and solvents were reagent grade and were used as received. For spectroscopic and electrochemical studies, HPLC-grade solvents were used.

UV/vis/near-IR spectroelectrochemical studies were performed in CH_3CN/0.1 M Bu_4NPF_6 at 298 K using an optically transparent thin-layer electrode cell[24] mounted in the sample compartment of a Bruins Instruments Omega 10 spectrophotometer. FT-IR spectra were taken on a Nicolet spectrophotometer with samples prepared as KBr pellets. The solution electrical conductivity was checked using a Systronic 305 conductivity bridge. ^{1}H NMR spectra were obtained with a 300 MHz Varian FT spectrometer. The EPR measurements were made in a two-electrode capillary tube[21] with an X-band Bruker system ESP300, equipped with a Bruker ER035 M gaussmeter and a HP 5350B microwave counter. Cyclic voltammetric measurements were carried out using a PAR model 273A electrochemistry system. Platinum wire working and auxiliary electrodes and an aqueous saturated calomel reference electrode (SCE) were used in a three-electrode configuration. The supporting electrolyte was Et_4NClO_4, and the solute concentration was approximately 10^{-3} M. The half-wave potential $E°_{298}$ was set equal to $0.5(E_{pa} + E_{pc})$, where E_{pa} and E_{pc} are anodic and cathodic cyclic voltammetric peak potentials, respectively. All experiments were carried out under a dinitrogen atmosphere. Elemental analysis was carried out with a Perkin-Elmer 240C elemental analyzer. Electrospray ionization mass (ESI MS) spectra were recorded on a Micromass Q-ToF mass spectrometer.

Synthesis of Complexes [{($\mathbf{L_{1-3}}$)$\mathbf{ClRu^{II}}$}$_2$(μ-tppz)] (1−3). The complexes **1**−**3** were made by using a general procedure. The details of [{(L_1)$ClRu^{II}$}$_2$(μ-tppz)] (**1**) are given below: The free AL HL_1 = 2-picolinic acid (38 mg, 0.31 mmol), excess LiCl (54 mg, 1.3 mmol), and NEt_3 (0.2 mL, 1.55 mmol) were added to the ethanolic solution (20 mL) of the starting complex [Cl_3Ru(μ-tppz)$RuCl_3$] (100 mg, 0.124 mmol). The mixture was heated at reflux for 5 h under a dinitrogen atmosphere. The initial greenish solution gradually changed to deep green. The solvent was then removed under reduced pressure. The dried crude product was purified by using a silica gel column. The green dinuclear complex **1** was eluted by a solvent mixture of CH_3CN/MeOH (4:1). Evaporation of the solvent under reduced pressure yielded pure complex **1**.

For the synthesis of **2** and **3**, the reaction mixture was heated to reflux for 12 h and the solvent mixtures CH_3CN/MeOH (4:1) and CH_3CN/MeOH (3:1), respectively, were used to eluate the pure products from the silica gel column.

For **1**. Yield: 51 mg (45%). Anal. Calcd (found) for $C_{36}H_{24}Cl_2N_8O_4Ru_2$: C, 47.69 (47.82); H, 2.67 (2.81); N, 12.37 (12.12). ESI MS (in CH_3CN). Calcd (found) for [**1**]$^+$: m/z 905.94 (905.95). ^{1}H NMR [$(CD_3)_2SO$, δ/ppm (J/Hz)]: 9.92 (d, 5.7, 1H), 8.87 (d, 7.8, 2H), 8.35 (t, 6.6/5.8, 1H), 8.19 (m, 4H), 7.99 (t, 8.1/7.5, 2H), 7.69 (t, 6.3/6.6, 2H). IR (KBr disk, νC(=O)O$^-$/cm^{-1}): 1631.

For **2**. Yield: 50 mg (40%). Anal. Calcd (found) for $C_{44}H_{28}Cl_2N_8O_4Ru_2$: C, 52.49 (52.36); H, 2.81 (2.68); N, 11.14 (11.24). ESI MS (in CH_3CN). Calcd (found) for [**2**]$^+$: m/z 1005.96 (1006.06). ^{1}H NMR [$(CD_3)_2SO$, δ/ppm (J/Hz)]: 10.31 (1H), 8.95 (d, 8.1, 1H), 8.85 (d, 7.8, 1H), 8.67 (m, 6H), 8.41 (m, 3H), 8.28 (m, 3H), 7.88 (m, 10H), 7.61 (1H), 7.33 (t, 7.5/7.8, 1H), 6.96 (t, 6.5, 1H). IR (KBr disk, νC(=O)O$^-$/cm^{-1}): 1630.

For **3**. Yield: 59 mg (47%). Anal. Calcd (found) for $C_{44}H_{28}Cl_2N_8O_4Ru_2$: C, 52.49 (52.59); H, 2.81 (2.86); N, 11.14 (11.38). ESI MS (in CH_3CN). Calcd (found) for [**3**]$^+$: m/z 1005.96 (1006.98). ^{1}H NMR [$(CD_3)_2SO$, δ/ppm (J/Hz)]: 10.48 (d, 4.8, 1H), 8.96 (d, 7.2, 1H), 8.83 (d, 7.8, 2H), 8.58 (d, 7.2, 1H), 8.5 (d, 8.4, 1H), 8.10 (d, 5.4, 1H), 8.07 (d, 5.4, 1H), 7.99 (t, 7.5, 2H), 7.87 (t, 7.8/7.5, 2H), 7.61 (m, 2H). IR (KBr disk, νC(=O)O$^-$/cm^{-1}): 1618.

Crystal Structure Determination. Single crystals were grown by slow evaporation of an acetonitrile solution of **1** and 1:1 mixtures of methanol/toluene and acetonitrile/hexane for **2** and **3**, respectively. The crystal data of **1**−**3** were collected on an Oxford X-CALIBUR-S CCD diffractometer at 150 K. Selected data collection parameters and other crystallographic results are summarized in Table 1. All data were corrected for Lorentz polarization and absorption effects. The program package of *SHELX-97*[25] was used for structure solution and full-matrix least-squares refinement on F^2. H atoms were included in the refinement using the riding model. The crystal structures of complexes **1a**, **2**, and **3** are shown in Figures 1−3. The asymmetric unit of **1** consists of two independent species (molecules **1a** and **1b**; **1b** is shown in Figure S2 in the SI), while the asymmetric unit of **3** is composed of half of the molecules because of the presence of a crystallographic inversion center. The crystallographic parameters and selected bond distances and angles for **1**−**3** are listed in Tables 1 and 2 and S1−S3 in the SI, respectively. Selected bond distances and angles of **1b** are given in Table S4 in the SI. The asymmetric units of the crystals of **1**−**3** contain one acetonitrile and three water molecules (**1**), one disordered toluene and four water molecules (**2**), and one *n*-hexane molecule (**3**). The H atoms associated with the water and toluene molecules in **2** and hexane molecule in **3** could not be located. The disordered toluene and *n*-hexane molecules in **2** and **3**, respectively, were refined isotropically.

The atomic coordinates for these structures have been deposited with the Cambridge Crystallographic Data Centre as CCDC numbers 760100, 760101, and 760102 for **1**−**3**, respectively. The coordinates can be obtained, upon request, from the Director, Cambridge Crystallographic Data Centre, 12 Union Road, Cambridge CB2 1EZ, U.K.

Computational Details. Full geometry optimizations were carried out using the DFT method at the (R)B3LYP level for **2**/**3** and (U)B3LYP for $\mathbf{2}^+$/$\mathbf{3}^+$ and $\mathbf{2}^-$/$\mathbf{3}^-$.[26] All elements except ruthenium were assigned the 6-31G(d) basis set. The SDD basis set with effective core potentials was employed for the Ru atom.[27] The vibrational frequency calculations were performed to ensure that the optimized geometries represent the local minima and there are only positive eigenvalues. All calculations were performed with the *Gaussian03* program package.[28] Vertical electronic

(24) Krejcik, M.; Danek, M.; Hartl, F. *J. Electroanal. Chem.* **1991**, *317*, 179.

(25) Sheldrick, G. M. *SHELX-97, Program for Crystal Structure Solution and Refinement*; University of Göttingen: Göttingen, Germany, 1997.

(26) Lee, C.; Yang, W.; Parr, R. G. *Phys. Rev. B* **1988**, *37*, 785.

(27) (a) Andrae, D.; Haeussermann, U.; Dolg, M.; Stoll, H.; Preuss, H. *Theor. Chim. Acta* **1990**, *77*, 123. (b) Fuentealba, P.; Preuss, H.; Stoll, H.; Szentpaly, L. V. *Chem. Phys. Lett.* **1989**, *89*, 418.

excitations based on B3LYP-optimized geometries were computed for **2**/**3**, $\mathbf{2}^{+}/\mathbf{3}^{+}$, and $\mathbf{2}^{-}/\mathbf{3}^{-}$ using the TD-DFT formalism[29] in acetonitrile using conductor-like polarizable continuum model.[30] *GaussSum*[31] was used to calculate the fractional contributions of various groups to each molecular orbital.

(28) Frisch, M. J.; Trucks, G. W.; Schlegel, H. B.; Scuseria, G. E.; Robb, M. A.; Cheeseman, J. R.; Montgomery, J. A. ; Vreven, T., Jr.; Kudin, K. N.; Burant, J. C.; Millam, J. M.; Iyengar, S. S.; Tomasi, J.; Barone, V.; Mennucci, B.; Cossi, M.; Scalmani, G.; Rega, N.; Petersson, G. A.; Nakatsuji, H.; Hada, M.; Ehara, M.; Toyota, K.; Fukuda, R.; Hasegawa, J.; Ishida, M.; Nakajima, T.; Honda, Y.; Kitao, O.; Nakai, H.; Klene, M.; Li, X.; Knox, J. E.; Hratchian, H. P.; Cross, J. B.; Bakken, V.; Adamo, C.; Jaramillo, J.; Gomperts, R.; Stratmann, R. E.; Yazyev, O.; Austin, A. J.; Cammi, R.; Pomelli, C.; Ochterski, J. W.; Ayala, P. Y.; Morokuma, K.; Voth, G. A.; Salvador, P. ; Dannenberg, J. J.; Zakrzewski, V. G.; Dapprich, S.; Daniels, A. D.; Strain, M. C.; Farkas, O.; Malick, D. K.; Rabuck, A. D.; Raghavachari, K.; Foresman, J. B.; Ortiz, J. V.; Cui, Q.; Baboul, A. G.; Clifford, S.; Cioslowski, J.; Stefanov, B. B.; Liu, G.; Liashenko, A.; Piskorz, P.; Komaromi, I.; Martin, R. L.; Fox, D. J.; Keith, T.; Al-Laham, M. A.; Peng, C. Y.; Nanayakkara, A.; Challacombe, M.; Gill, P. M. W.; Johnson, B.; Chen, W.; Wong, M. W.; Gonzalez, C.; Pople, J. A. *Gaussian 03*; Gaussian, Inc.: Wallingford, CT, 2004.

(29) (a) Bauernschmitt, R.; Ahlrichs, R. *Chem. Phys. Lett.* **1996**, *256*, 454. (b) Stratmann, R. E.; Scuseria, G. E.; Frisch, M. J. *J. Chem. Phys.* **1998**, *109*, 8218. (c) Casida, M. E.; Jamorski, C.; Casida, K. C.; Salahub, D. R. *J. Chem. Phys.* **1998**, *108*, 4439.

(30) (a) Barone, V.; Cossi, M. *J. Phys. Chem. A* **1998**, *102*, 1995. (b) Cossi, M.; Barone, V. *J. Chem. Phys.* **2001**, *115*, 4708. (c) Cossi, M.; Rega, N.; Scalmani, G.; Barone, V. *J. Comput. Chem.* **2003**, *24*, 669.

(31) O'Boyle, N. M.; Tenderholt, A. L.; Langner, K. M. *J. Comput. Chem.* **2008**, *29*, 839.

Acknowledgment. Financial support received from the Department of Science and Technology (DST, New Delhi, India) and the DAAD, FCI, and DFG (Germany) is gratefully acknowledged. X-ray structural studies for **1**−**3** were carried out at the National Single Crystal Diffractometer Facility, Indian Institute of Technology, Bombay, India. Special acknowledgment is made to the Sophisticated Analytical Instrument Facility (SAIF), Indian Institute of Technology, Bombay, India, for providing the NMR facility.

Supporting Information Available: X-ray crystallographic files in CIF format for **1**−**3**, a general molecular sketch (Scheme S1), mass spectra of **1**−**3** (Figure S1), ORTEP diagram of **1b** (Figure S2), crystal structure perspectives along the Ru---Ru axis (Figure S3), nonplanarity of the pyrazine ring of tppz in the crystal structures (Figure S4), DFT-optimized structures of **2** and **3** (Figure S5), packing diagrams of **1** and **2** (Figures S6 and S7), UV/vis/near-IR spectroelectrochemistry of **2** and **3** (Figures S8 and S9), EPR spectra of $\mathbf{1}^{-}$−$\mathbf{3}^{-}$ (Figure S10), structural parameters of **1**−**3** (Tables S1−S6), and DFT data for **2** and **3** (Tables S7−S14). This material is available free of charge via the Internet at http://pubs.acs.org.